HANDBOOK OF PLASMA IMMERSION ION IMPLANTATION AND DEPOSITION

Edited by

André Anders

Lawrence Berkeley National Laboratory

A WILEY-INTERSCIENCE PUBLICATION

JOHN WILEY & SONS, INC.

New York / Chichester / Weinheim / Brisbane / Singapore / Toronto

This book is printed on acid-free paper. ♾

Copyright © 2000 by John Wiley & Sons. All rights reserved.

Published simultaneously in Canada.

No part of this publication may be reproduced, stored in a retrieval system or transmitted in any form or by any means, electronic, mechanical, photocopying, recording, scanning or otherwise, except as permitted under Section 107 or 108 of the 1976 United States Copyright Act, without either the prior written permission of the Publisher, or authorization through payment of the appropriate per-copy fee to the Copyright Clearance Center, 222 Rosewood Drive, Danvers, MA 01923, (508) 750-8400, fax (978) 750-4744. Requests to the Publisher for permission should be addressed to the Permissions Department, John Wiley & Sons, Inc., 605 Third Avenue, New York, NY 10158-0012, (212) 850-6011, fax (212) 850-6008, E-Mail: PERMREQ@WILEY.COM.

For ordering and customer service, call 1-800-CALL-WILEY.

Library of Congress Cataloging-in-Publication Data:

Handbook of plasma immersion ion implantation and deposition / André Anders, editor.
p. cm.
Includes bibliographical references and indexes.
ISBN 0-471-24698-0 (cloth : alk. paper)
1. Ion implantation. 2. Ion bombardment—Industrial applications. 3. Plasma (Ionized gases)—Industrial applications. 4. Metals—Surfaces. 5. Metals—Finishing. I. Anders, André.

TS695.25.H36 2000
671.7—dc21 99-089627

Printed in the United States of America.

10 9 8 7 6 5 4 3 2 1

6

DESIGN OF A PIII&D PROCESSING CHAMBER

Jesse Matossian, George A. Collins, Paul K. Chu,
Carter P. Munson, and Joseph V. Mantese

6.1 INTRODUCTION

A complete facility for conducting plasma source ion implantation (PSII), plasma immersion ion implantation (PIII), and plasma immersion implantation and deposition (PIIID), in this book generically referred to as PIII&D, is comprised of three elements shown schematically in Figure 6.1. These are the processing chamber, the plasma generator and material source, and the pulse-power modulator. In this chapter we will review the features and requirements for the design of the processing chamber. Reviews of plasma generators (including sources of material) and pulse-power modulators follow in Chapters 7 and 8, respectively.

This review of the processing chamber design will focus on two major areas of PIII&D technology: tribological coatings and implantation and semiconductor processing. The features of processing chambers required for these two applications depend on several factors; no single design can suit the needs for both applications. For example, the design of a processing chamber used to conduct a 100-kV, 50-kW (average power) implant of nitrogen ions at a dose of 4×10^{17} ions/cm^2 into a 1500-kg metal die will differ markedly from the design

Handbook of Plasma Immersion Ion Implantation and Deposition, Edited by André Anders
ISBN 0-471-24698-0 © 2000 John Wiley & Sons, Inc.

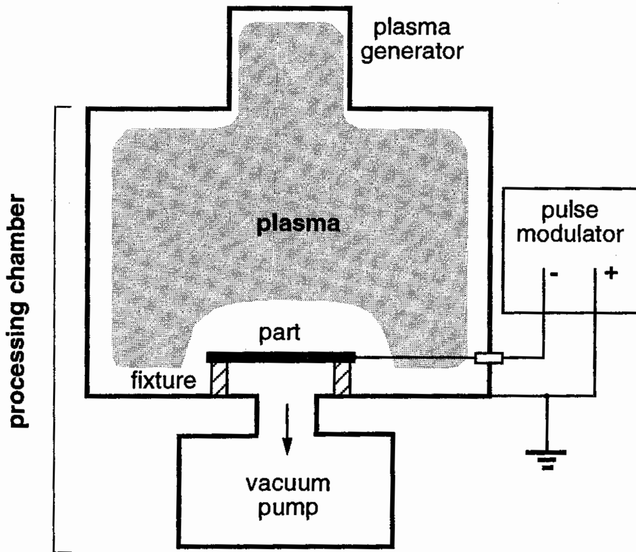

Figure 6.1 Schematic diagram of the three elements of a PIII&D processing chamber.

of a processing chamber used to conduct a 5-kV, 0.5-kW (average power) implant of boron ions at a dose of 4×10^{15} ions/cm^2 into silicon wafers.

The engineer designing a PIII&D processing chamber is required to combine the disciplines of vacuum and plasma technology, surface and materials science, process control, and mechanical engineering with economic and process issues that are related to the specific application. These disciplines and issues will be reviewed, first learning from existing processing chambers, and then this background will be used to provide the PIII&D engineer with guidelines to aid in the design of new facilities for advanced applications.

6.2 BACKGROUND

The design of a PIII&D processing chamber can be linked to several interdependent elements that are described schematically in Figure 6.2. The processing chamber design and all of the elements that comprise it depend on the PIII&D application. The PIII&D application consists of three elements: the type and size of parts to be treated, the type of treatment to be performed, and the throughput of parts. The processing chamber design can be divided into two separate levels. The first-level design elements, which can be linked to the three PIII&D applications elements described above, are the vacuum chamber size and type, the implantation voltage, and the processing power. Specifically, the type and size of parts to be treated help to define the vacuum chamber size that must be used. The type of treatment to be performed defines the

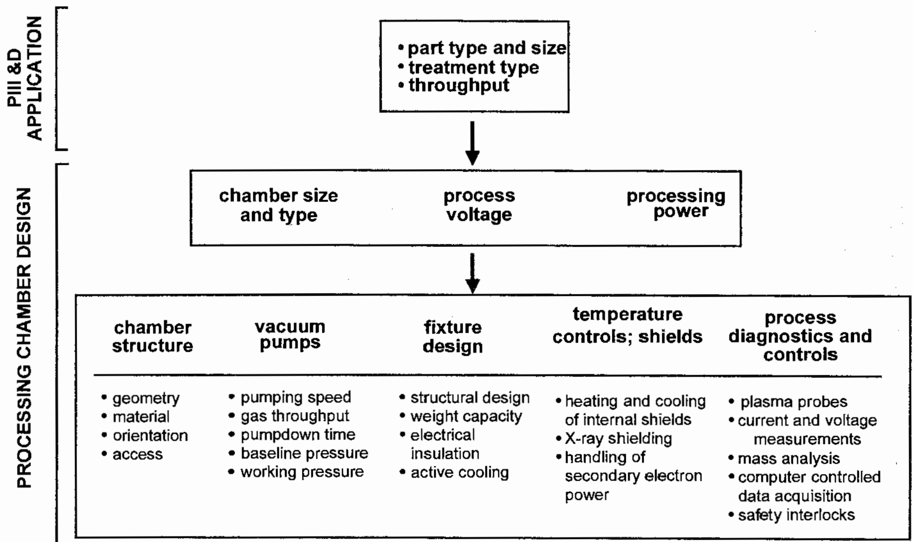

Figure 6.2 Elements that affect the processing chamber design for a PIII&D system.

implantation voltage, and the throughput defines the processing power, as well as the vacuum chamber type (i.e., batch chamber or continuous-flow chamber).

The second level of the processing chamber design consists of five elements: the chamber structure, vacuum pumps, fixture design, temperature control and shielding, and process diagnostics and controls. These are linked to the three, first-level design elements described above (Fig. 6.2).

6.3 GENERAL TRENDS FOR CHAMBER SIZE, VOLTAGE, AND PROCESSING POWER

From a survey of existing process facilities, several general trends can be established for the three first-level processing design elements that will play a fundamental role in the design guidelines and scaling relationships. Figure 6.3 shows the variation of the processing chamber size for existing facilities with tribology and semiconductor applications. The average chamber size used for the tribological treatment of parts is about 1 m^3. This is 20 times greater than the average chamber size of 0.05 m^3 used for semiconductor treatments of parts; the transition size is about 0.2 m^3. The correlation of chamber size and application partially relates to the fact that parts treated in tribological applications are three dimensional and therefore many times larger in volume than parts treated in semiconductor applications, which are two dimensional. However, it also has to do with the fact that higher implantation voltage and processing power are used in the tribological treatment of parts. Note that

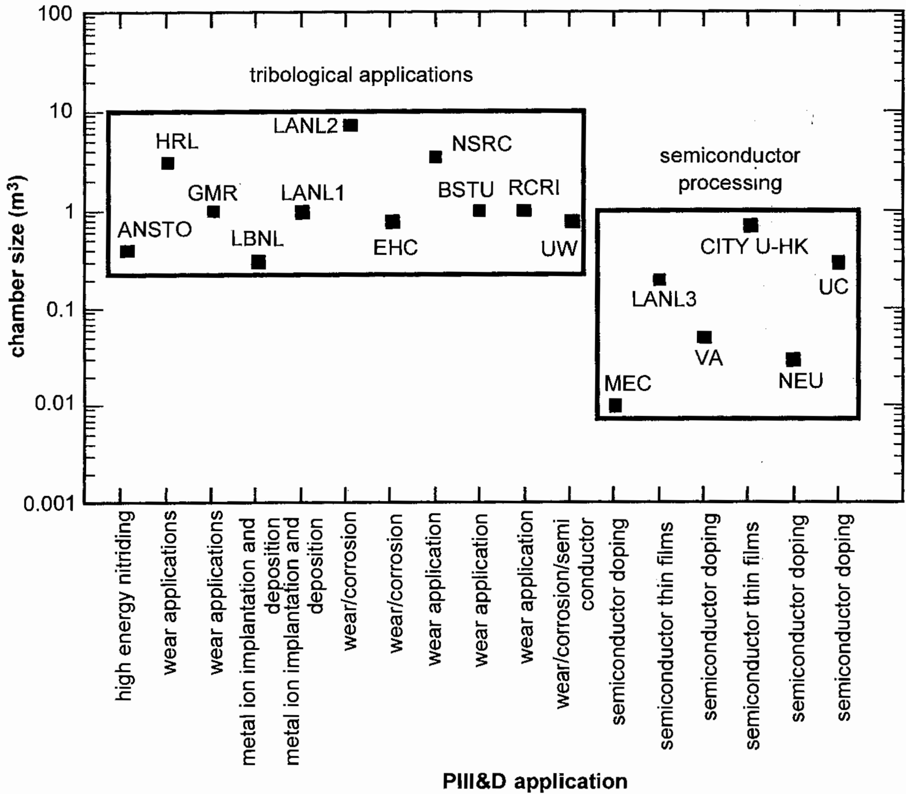

Figure 6.3 Variation of chamber size with application for PIII&D facilities in use throughout the world (data from [1–15]). Table 6.1 lists the facility designations used.

these statements have been derived from existing facilities that are usually designed for research purposes. Batch processing under industrial conditions will require larger chambers not only for tribological but also for semiconductor processing [current semiconductor research and development (R&D) facilities usually handle one wafer at a time, with wafer sizes up to 300 mm diameter).

Figure 6.4 shows the variation of implantation voltage with application for the same facilities presented in Figure 6.3. The average implantation voltage used for the tribological treatments of parts is about 70 kV, which is 10 times greater than the average implantation voltage of 7 kV used for semiconductor processing. The transition voltage is about 10 kV, which is about the minimum voltage that can be used to modify the tribological properties of materials, and the maximum voltage that can be used to do shallow-depth implants of dopants into semiconductors. Of course, many tribological applications use relatively low voltages (particularly ion nitriding and ion-assisted deposition),

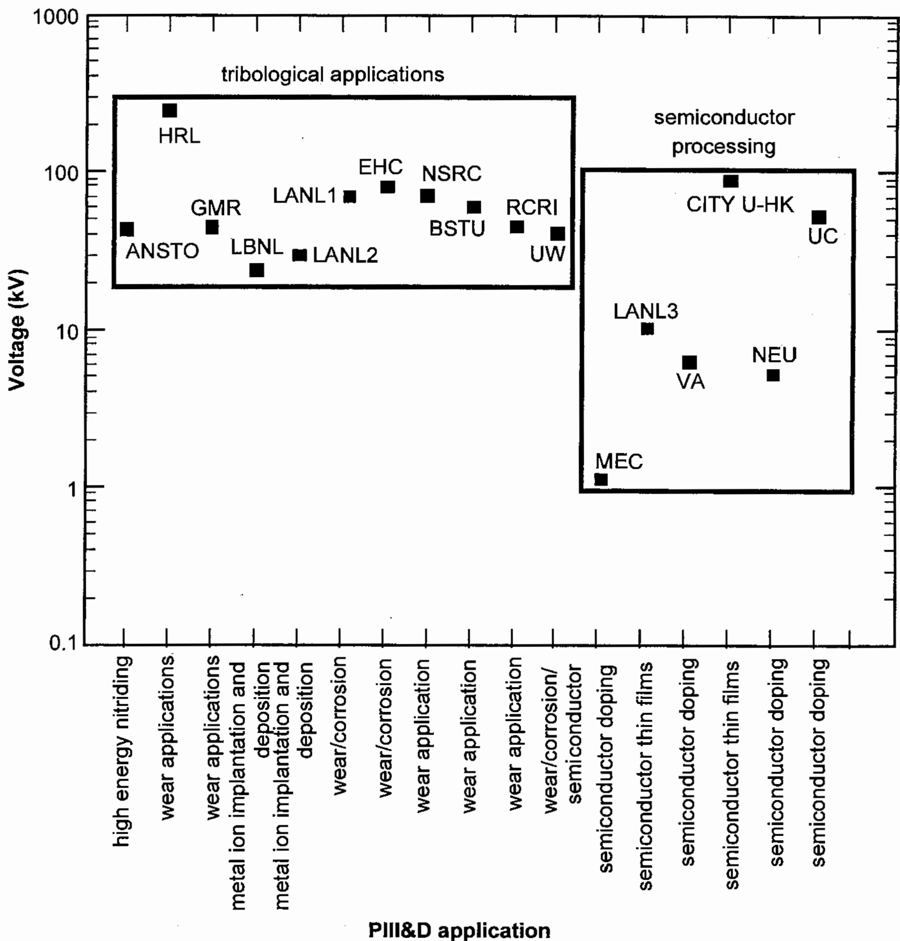

Figure 6.4 Variation of implantation voltage with application for PIII&D facilities in use throughout the world.

and some semiconductor applications (particularly SPIMOX) use relatively high voltages.

Figure 6.5 shows the variation of processing power with application for a similar range of facilities presented in Figures 6.3 and 6.4 (see Table 6.1 for definitions of the facility designations). Processing power is defined as the product of voltage and average current provided by the pulse modulator. The average processing power used in the systems shown in Figure 6.5 for tribological applications is about 10 kW, which is over 100 times greater than the average processing power of 0.1 kW used for semiconductor applications. For tribological treatments of parts, higher voltages are used and parts have larger surface area, thus requiring higher total currents. Also important is the

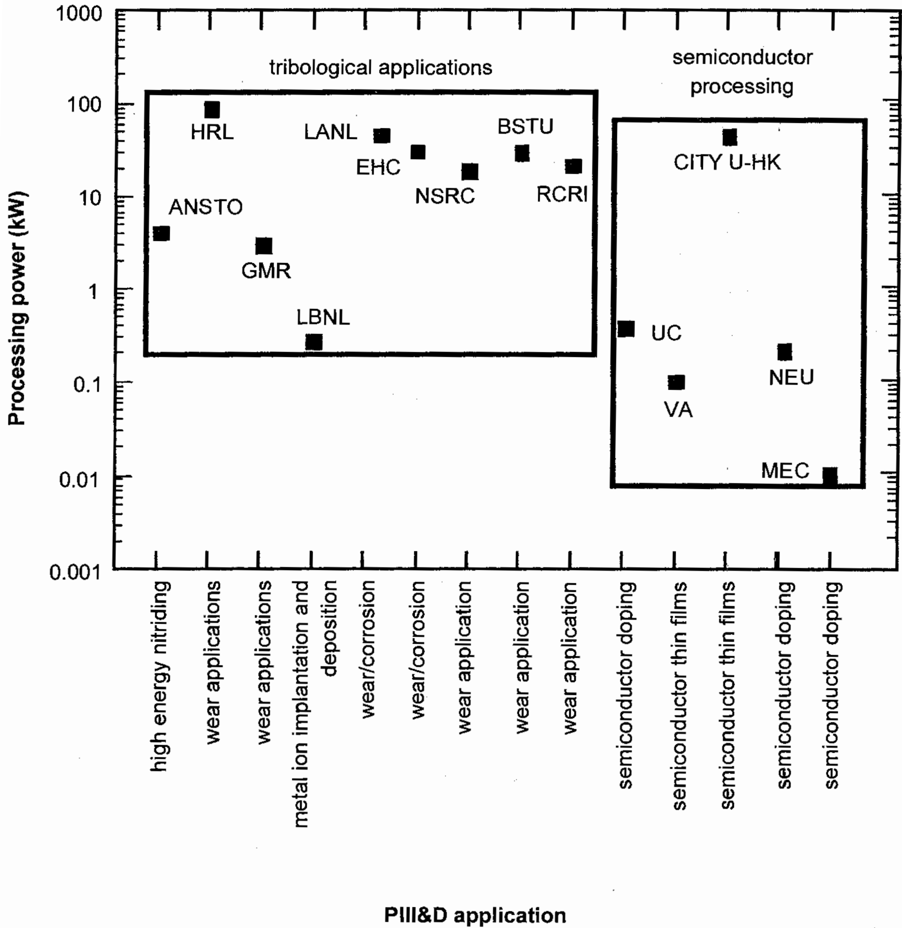

Figure 6.5 Variation of processing power with application for PIII&D facilities in use throughout the world.

higher implanted dose typically required for tribological treatments. This generally means higher powers are required to achieve the dose in a reasonable time, within the limitations imposed by the thermal power that can be tolerated by the parts. As with chamber size, the requirements on processing power will change when going from research to industrial batch processing of parts.

It is instructive to show representative examples of chambers that illustrate the range in size, voltage, and processing power for the facilities considered in Figures 6.3, 6.4, and 6.5. With respect to chamber size, the reader is referred to Figure 1.13, which shows the large-scale, 8-m^3 PIII facility at Los Alamos National Laboratory used for tribological applications [1]. Figure 6.6 shows the small-scale, 0.94-m^3 R&D facility at the City University of Hong Kong [2, 16] designed for the fabrication of novel materials, including semiconductors.

Table 6.1 Definitions of the facility designations used in Figures 6.3, 6.4, and 6.5

ANSTO	Australian Nuclear Science and Technology Organisation, Lucas Heights, Australia
BSTU	Bauman State Technical University, Moscow, Russia
City U-HK	City University of Hong Kong, Kowloon, Hong Kong
EHC	Empire Hard Chrome, Inc., Chicago, Illinois, United States
GMR	General Motors Research, Warren, Michigan, United States
HRL	HRL Laboratories, LLC, Malibu, California, United States
LBNL	Lawrence Berkeley National Laboratory, Berkeley, California, United States
LANL	Los Alamos National Laboratory, Los Alamos, New Mexico, United States
MEC	Matsushita Electric Industrial Co., Ltd., Osaka, Japan
NSRC	North Star Research Corporation, Albuquerque, New Mexico, United States
NEU	Northeastern University, Boston, Massachusetts, United States
RCRI	Research Center Rossendorf, Inc., Dresden, Germany
UC	University of California, Berkeley, California, United States
UW	University of Wisconsin, Madison, Wisconsin, United States
VA	Varian Associates, Palo Alto, California, United States

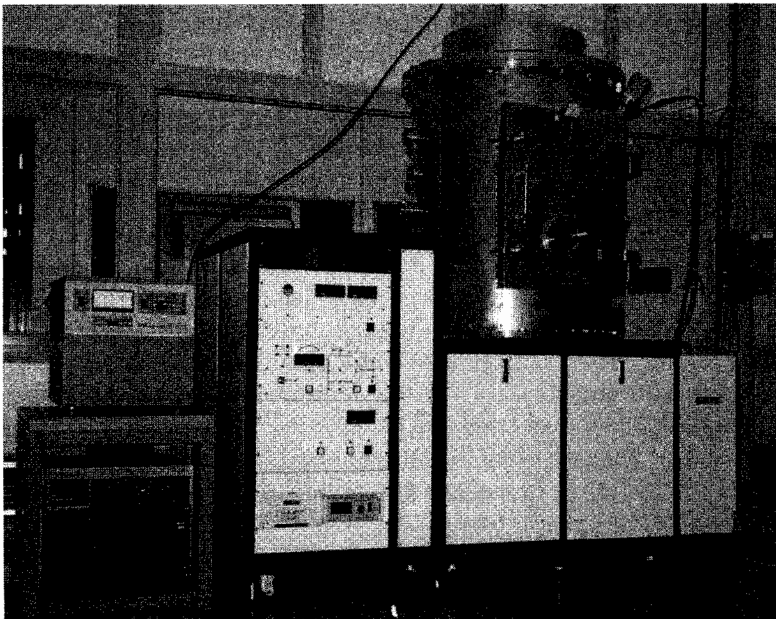

Figure 6.6 Photograph of the 0.94-m^3 R&D facility at City University of Hong Kong.

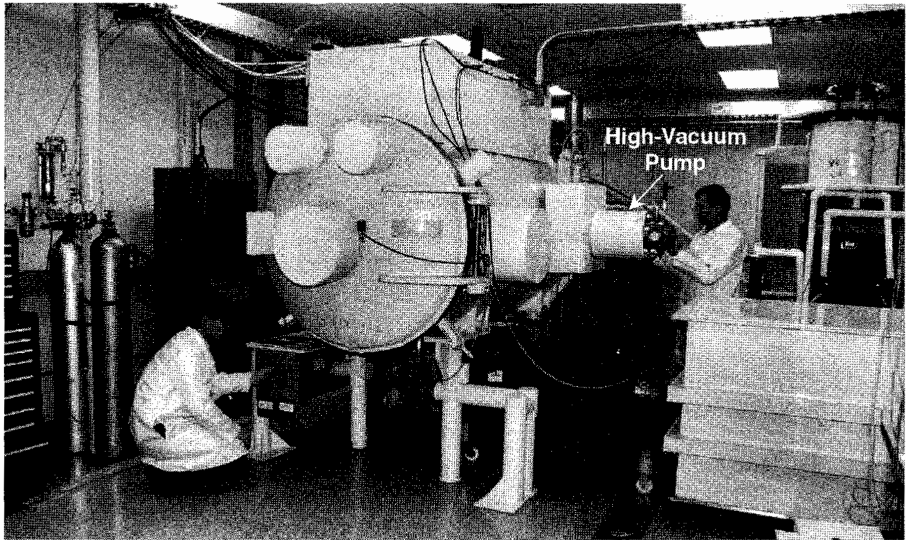

Figure 6.7 Photograph of the 250-kV, 100-kW tribology facility at Hughes Research Laboratories.

With respect to high voltage and power, Figure 6.7 shows the 250-kV, 100-kW facility at Hughes Research Laboratories (HRL) used for tribological implants [3, 17].

6.4 DESIGN GUIDELINES AND SCALING RELATIONSHIPS FOR PIII&D CHAMBERS

6.4.1 Chamber Size

In this section, we develop a set of design guidelines and scaling relationships for the first-level processing chamber design elements as defined in Figure 6.2. We use a one-dimensional analysis for the treatment of a single part that is based on simple physical arguments to quantitatively correlate processing chamber size with implantation voltage. Processing power is considered later. Although actual vacuum chambers are three dimensional and typically involve the treatment of multiple three-dimensional parts, the simple one-dimensional analysis of the treatment of a single part will be shown to provide results that agree remarkably well with the design and scaling of actual chambers.

A schematic diagram of a one-dimensional vacuum chamber is shown in Figure 6.8. The overall dimension of the vacuum chamber must be equal to or exceed the sum of the dimensions of the plasma reservoir, the sheath at the end of an applied voltage pulse, the part to be treated, and the fixture that supports

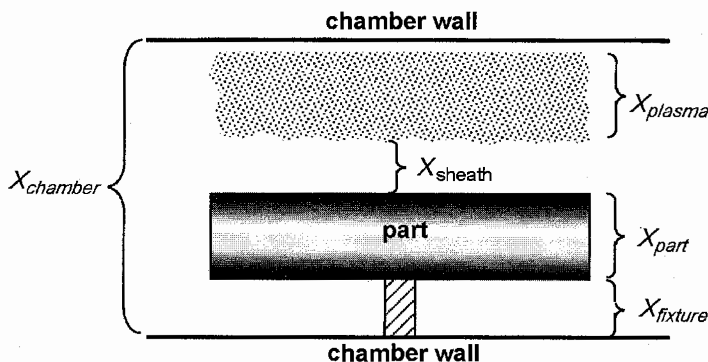

Figure 6.8 Schematic diagram of a one-dimensional vacuum chamber.

the part from the vacuum chamber wall:

$$X_{\text{chamber}} \geq X_{\text{plasma}} + X_{\text{sheath}} + X_{\text{part}} + X_{\text{fixture}} \tag{6.1}$$

Note that the sheath dimension, X_{sheath}, is not given by the initial ion matrix sheath but by the final thickness of the sheath at the end of the high-voltage pulse (Section 4.2). Through the sheath dimension, Eq. (6.1) links chamber size and PIII&D voltage.

We will evaluate Eq. (6.1) by inserting the various dimensions that are characteristic of tribological and semiconductor processing. A combination of empirically obtained and theoretically derived values will be used.

The *fixture dimension* is obtained empirically and depends greatly on the voltage used. It is almost independent of the part size. From Figure 6.4, the average implantation voltages characterizing tribological and semiconductor processing are 70 and 7 kV, respectively. As will be discussed in Section 6.6.2, a fixture dimension of approximately 0.1 m is adequate to provide sufficient electrical isolation from the chamber walls at 70 kV. This dimension could be greater than 0.1 m, however, it can be adequate for voltages as high as 100 kV. Similarly, at 7 kV, the fixture dimension can be down-scaled linearly to 0.01 m. As a general rule of thumb, the isolation gap can be determined by:

$$X_{\text{fixture}} \geq 1.5\,\text{mm/kV} \times U\ (\text{kV}) \tag{6.2}$$

The *part dimension* for semiconductor processing is of order 1 mm (thickness of wafers). For tribological applications, the part dimension can range from a few centimeters to about 1 m. For this simple analysis, we will use an average part dimension of about 0.3 m.

The *sheath dimension* must be determined using the theoretical analysis of Section 4.2. In the simplest case, one can use the sheath thickness [Eq. (4.2.4)] derived from the Child–Langmuir law in planar geometry, which is rewritten

here as:

$$X_{\text{sheath}}(t) = X_0 \sqrt[3]{\frac{2}{3}\omega_{\text{pi}} t + 1} \tag{6.3}$$

where t is the time within the pulse duration, ω_{pi} is ion plasma frequency, $X_0 = \sqrt{2\varepsilon_0 V / e n_0}$ is the thickness of the ion matrix sheath, V is the applied implantation voltage, and n_0 is the plasma density. For a sheath width of nonplanar geometry see Section 4.2.3.1.

As an example we consider a pulse of 10 μs duration. Figure 6.9 shows the variation of the sheath dimension in planar geometry as a function of voltage for three constant values of plasma density: $n_0 = 10^9$, 10^{10}, and $10^{11}\,\text{cm}^{-3}$. These densities are typical of those encountered in practice. The vertical dashed line in Figure 6.9 represents the arbitrary transition voltage of 10 kV, which distinguishes tribological from semiconductor applications. It should be noted that we have assumed that the sheath expands according to Eq. (6.3) during the entire pulse duration. In reality, the sheath expands until the Bohm criterion is satisfied or the plasma is exhausted from the entire chamber volume. The design engineer is advised to calculate the sheath thickness for the specific conditions as described in Section 4.2, taking into account possible plasma exhaustion and sheath refill times.

We can use Eq. (6.3) and Figure 6.9 to estimate the sheath dimension for use in Eq. (6.1). We use plasma densities and implantation voltages that are

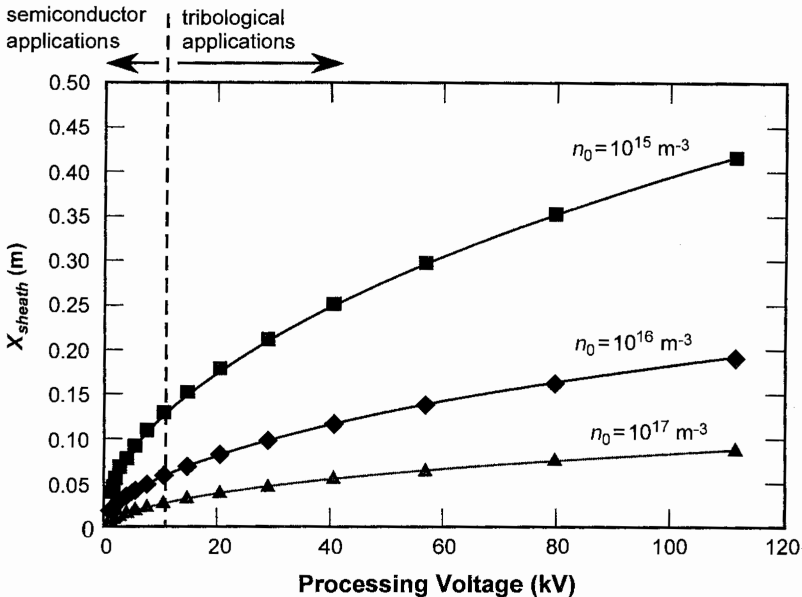

Figure 6.9 Variation of the sheath dimension in planar approximation as a function of bias voltage for constant values of plasma density.

representative of the specific application. For tribological applications we select an average implantation voltage of 70 kV and find a sheath dimension of about 0.3 m for a plasma density of $10^9\,\mathrm{cm}^{-3}$. This is representative for existing tribology facilities operating at this voltage [1, 18]. Similarly, for semiconductor applications, we select the average implantation voltage of 7 kV and sheath dimension of 2.5 cm for a plasma density of $10^{11}\,\mathrm{cm}^{-3}$ [4, 19].

The plasma dimension is the last input required for Eq. (6.1). Empirically, a plasma dimension of 0.3 m is recommended for either application, regardless of the part size. This value is recommended to have a plasma reservoir that can provide the ion flux during sheath expansion and "refills" the sheath after each voltage pulse.

In summary, for tribology applications, Eq. (6.1) reads $X_{\mathrm{chamber}} \geq 0.3\,\mathrm{m} + 0.3\,\mathrm{m} + 0.3\,\mathrm{m} + 0.1\,\mathrm{m} \approx 1\,\mathrm{m}$. Therefore, to conduct 70-kV PIII implants of 0.3-m-thick parts, the one-dimensional vacuum chamber dimension should be on the order of 1 m, or about $1\,\mathrm{m}^3$ in volume, assuming that the same analysis is valid for each dimension. Indeed, this chamber volume agrees well with the average chamber volume of $1\,\mathrm{m}^3$ for existing tribological facilities (Fig. 6.3).

Analogously we obtain for semiconductor PIII&D $X_{\mathrm{chamber}} \geq 0.3\,\mathrm{m} + 0.025\,\mathrm{m} + 0.001\,\mathrm{m} + 0.01\,\mathrm{m} \approx 0.34\,\mathrm{m}$. Therefore, to conduct 7-kV ion implantation into wafers, the one-dimensional chamber size should be about 0.34 m, which corresponds to $0.04\,\mathrm{m}^3$ in volume, assuming that the same analysis is valid for each dimension. Also, this estimated chamber volume agrees well with the average chamber volume of $0.05\,\mathrm{m}^3$ for existing semiconductor facilities (Fig. 6.3).

It is instructive to demonstrate the application of Eq. (6.1) to an actual PIII&D vacuum chamber. Figure 6.10 shows the interior of the HRL tribology facility shown previously in exterior view in Figure 6.7. The facility consists of a horizontally oriented, cylindrical cross-section chamber and a flat-table fixture. The overall chamber diameter is 1.2 m. The fixture table has been positioned to provide the capability to treat parts having an average lateral dimension of 0.76 m and an average thickness of 0.2 m. In order to have a 100-kV electrical insulation gap for the fixture, the table is located about 0.3 m above the bottom of the chamber. This dimension is measured along the center diameter and is less near the perimeter of the chamber as shown in the figure. The HRL facility nominally operates at 100 kV with a plasma density of $n_0 = 10^9\,\mathrm{cm}^{-3}$. Using Figure 6.9, the computed sheath dimension at the end of a 10-μs pulse is 0.4 m. Thus Eq. (6.1) reads for this example $X_{\mathrm{chamber}} = 0.3\,\mathrm{m} + 0.4 + 0.2\,\mathrm{m} + 0.3\,\mathrm{m} = 1.2\,\mathrm{m}$, which agrees with the actual chamber dimension.

6.4.2 Chamber Structure

The structure elements of a vacuum chamber are defined in Figure 6.2. They include geometry, orientation, material composition, and the type of access. The chamber geometry can be cylindrical, square, rectangular, or bell shaped,

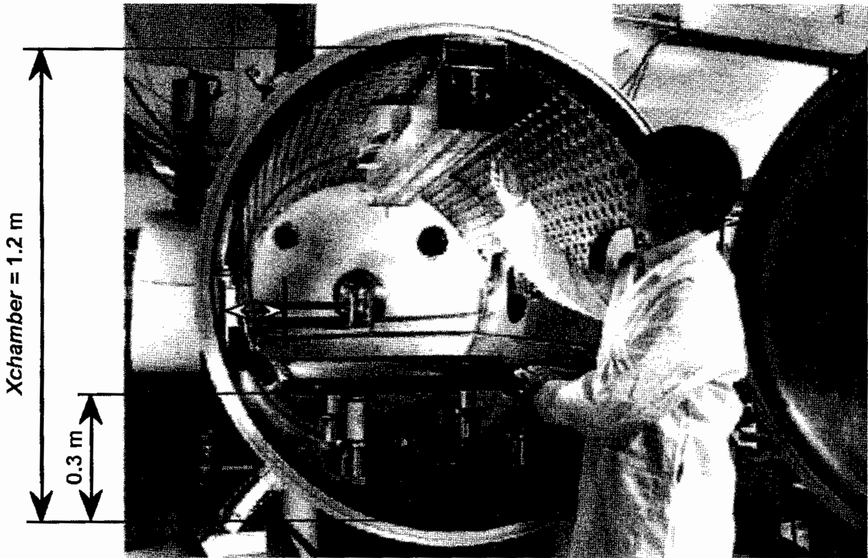

Figure 6.10 Photograph of the interior of the HRL tribology facility.

for example. The chamber can be oriented horizontally or vertically. The chamber can have front, rear, or bottom access for loading and unloading of parts, and it may have a hinged door, flange, or gate valve.

All PIII&D vacuum chamber facilities presently in use throughout the world are single-chamber, batch units. For large-scale parts, or limited numbers of small-scale parts, a batch-type chamber is the optimal way to treat parts. Even semiconductor cluster tools are essentially single-wafer batch processing units. In this chapter, we will not discuss continuous-flow chambers since their use for tribological or semiconductor processing is not practiced or considered at present.

Chambers of cylindrical geometry have the widest usage in PIII&D. They are prevalent in both tribological and semiconductor applications. A cylindrical geometry allows for straightforward scaling to large-size chambers with good structural integrity. Chambers can be either vertically or horizontally oriented. Access to the chamber interior may be provided manually, by the use of a cart, hoist, or forklift through either the front, the rear, the front and rear, or the side or bottom of the chamber via bolted flanges or via hinged doors. Figures 1.13 and 6.7 are examples of horizontally oriented, cylindrical chambers, while Figure 6.6 shows an example of a vertically oriented, cylindrical chamber.

Depending on the application, vertically oriented, cylindrical vacuum chambers may offer advantages over horizontally oriented chambers. For example, for vertically oriented chambers using bottom-load access, the operator has 360° access to the load in the retracted position. However, the chamber needs

to be lifted by a hoist to load and unload parts from the chamber bottom, and therefore as the part size increases, vertical height required of the room that houses the chamber becomes a limitation of this approach. For large chamber sizes ($\gg 1\,m^3$) the requirement of the hoist to lift the entire chamber becomes an issue. This is mitigated to some extent in the side-load approach shown in Figure 6.6, where parts are loaded into the chamber through a hinged door.

Square-geometry vacuum chambers also have use for PIII&D applications. This type of chamber is illustrated in Figure 6.11, which shows a photograph of the exterior of the 1-m^3 square-geometry tribology chamber at General Motors Research [5]. Square-geometry vacuum chambers make the most optimal use of the chamber interior volume when treating individual, large-scale parts

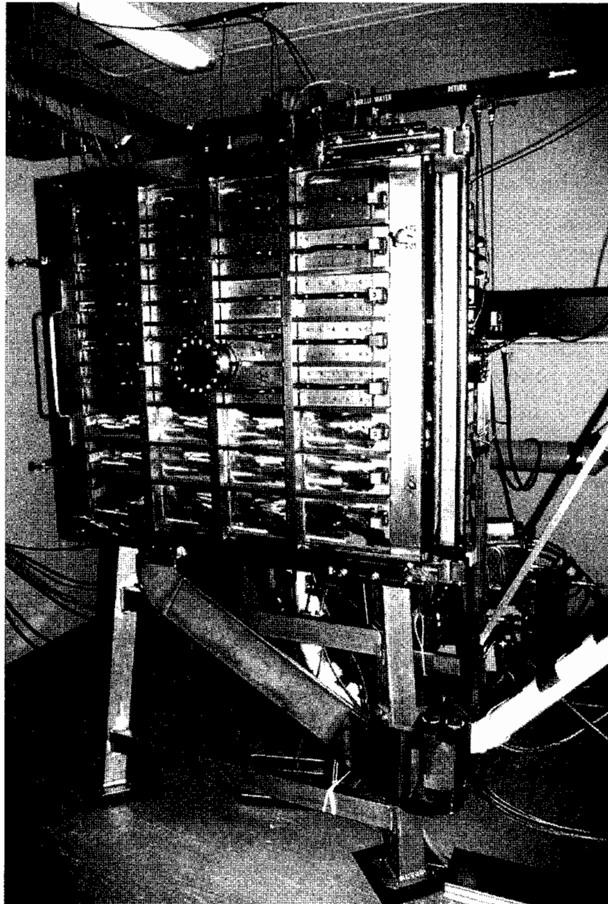

Figure 6.11 Photograph of the 1-m^3 square-geometry vacuum chamber used at General Motors Research.

with rectangular geometry or when packing-density issues must be addressed. However, scaling of large square-geometry chambers involves more complex structural issues compared to cylindrical chambers. Horizontal and vertical structural reinforcement must be used on each wall of the chamber, as shown in Figure 6.11. Access to the interior of the chamber is by front, rear, or front and rear hinged doors.

6.4.3 Chamber Material

There are basically three types of materials that can be used for vacuum chambers: stainless steel, carbon steel, and aluminum [20]. These are the same materials used in conventional plasma processing chambers, so we will only review the salient features of these materials as they apply to PIII&D applications.

While aluminum offers an advantage of being lightweight, it readily reacts with oxygen and water vapor and is difficult to clean and maintain clean. Aluminum is nonmagnetic, it is easily machined, but it is also easy to scratch, which limits its use for vacuum-sealing surfaces such as O-ring grooves. Compared to stainless steel and carbon steel, aluminum does not have sufficient strength for use in large-scale vacuum chambers ($\gg 1\ m^3$). For these reasons, aluminum vacuum chambers are limited in their use of PIII&D applications to small-size chambers ($< 1\ m^3$).

Carbon steel is a material that is easy to weld and inexpensive compared to stainless steel. It is a magnetic material, which may be of use in closing or shunting magnetic field lines for plasma confinement. Carbon steel easily rusts, and therefore care must be taken in its use where oxide contamination of internal vacuum chamber surfaces is a concern. The outgassing rate of carbon steel is about two orders of magnitude higher than that of stainless steel, which may not be compatible with many low-impurity vacuum applications of PIII&D such as semiconductor processing.

Stainless steel is a dense material with high strength, allowing for scaling of vacuum chambers to large sizes. It has excellent corrosion resistance properties, it can be baked out to desorb impurity gases, and it is easy to weld. Virtually all of the PIII&D chambers used are fabricated of stainless steel. As specific examples, the vacuum chambers shown in Figures 1.13, 6.6, and 6.7 use stainless steel for the structural material of the chamber. As shown below and in Chapter 9, stainless steel is also a good choice for shielding the X rays produced by the PIII&D process.

6.5 VACUUM PUMPS

6.5.1 Pumping Stages

Vacuum pumps are one of the most important processing chamber design elements because their performance affects the quality of the vacuum as well as

the stability of the process. It is therefore critical that the PIII&D technologist understand the fundamentals of vacuum technology as it applies to PIII&D technology.

There are three stages of operation for the pumping characteristics of a PIII&D processing chamber (Figure 6.12):

1. In the roughing stage, the chamber is typically pumped down to an intermediate pressure of order 10 Pa (0.1 Torr) using a mechanical pump, preparing the chamber for further evacuation by a high-vacuum pump.
2. During the high-vacuum pumping stage, the chamber is evacuated to the base pressure, typically 10^{-4} to 10^{-5} Pa (10^{-6} to 10^{-7} Torr).
3. The third stage depends on the specifics of the plasma source used for PIII&D. Some processes are done at vacuum base pressure, such as cathodic arc PIIID, but most processes require backfilling of the chamber with a processing gas. Even in the latter case, the chamber is often pumped using the high-vacuum pump.

We will focus on high-vacuum pumping and the pumping characteristics for the process stage with processing gas. For other information the reader is referred to the standard literature on vacuum technology such as [21, 22].

6.5.2 Relation of Pumping Speed, Outgassing, and Pressure

Under the conditions of constant outgassing of the chamber walls and the parts to be treated, the chamber pressure during the high-vacuum pumping stage is described by the well-known relation [23]

$$p(t) = p_{\mathrm{base}} + (p_1 - p_{\mathrm{base}}) \exp(-St/V) \tag{6.4}$$

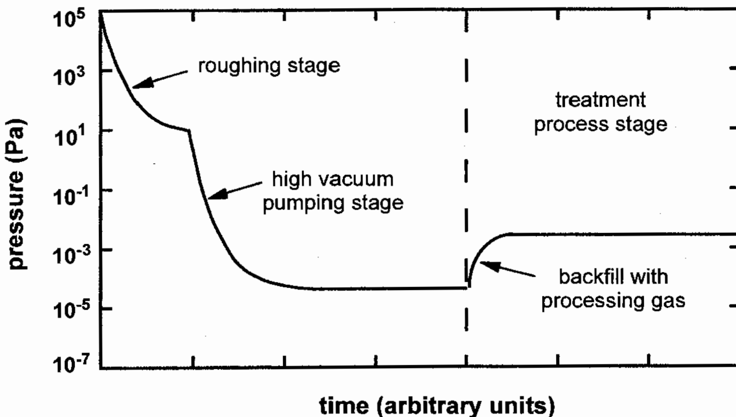

Figure 6.12 Three stages of operation of pumping hardware for a PIII&D processing chamber.

where t is the elapsed time, V is the processing chamber volume, S is the effective pumping speed of the high-vacuum pump at the chamber, p_1 is the chamber pressure at the end of the roughing stage, and p_{base} is the base pressure. The base pressure is related to the high-vacuum pumping speed and the outgassing rate, Q_{out} by the relation

$$p_{base} = Q_{out}/S \tag{6.5}$$

When the base pressure is reached (i.e., for t large), the pumping speed of the high-vacuum pump can be uniquely determined from Eq. (6.5) if the outgassing rate of the chamber walls and the parts is known.

The chamber operating pressure p_{op}, the high-vacuum pumping speed S, and operating gas throughput Q_{op} are linked in the treatment process stage to the functional form of Eq. (6.5):

$$p_{op} = Q_{op}/S \tag{6.6}$$

We will use Eq. (6.6) to compute the gas throughput requirement of the high-vacuum pump since the operating pressure and pumping speed are known quantities.

6.5.3 Determination of the High-Vacuum Pumping Speed

Equation (6.5) uniquely defines the effective pumping speed that is needed for given values of the base pressure and the outgassing rate. The outgassing rate is a fundamental process parameter that is difficult to obtain. In practice, one uses the nominal pumping speed value provided by the pump manufacturer and measures the base pressure for the determination of the effective outgassing rate via Equation (6.5).

To determine the desired effective pumping speed of a high-vacuum pump, one would use pumping performance nomographs provided by the pump manufacturer [24]. It typically requires the input of the base pressure, the desired pumpdown time, the volume of the chamber being pumped, and the outgassing rate of the chamber material.

The effective pumping speed can be determined using Eq. (6.5). Consider a chamber having an internal surface area, A_{ch}, and parts with the surface area A_{part} (in meters squared). If the chamber has been pumped down to its base pressure p_{base} (in Pascals), using the high-vacuum pumping system with a pumping speed S (in liters per second), there is equilibrium between the outgassing rate of the chamber walls and parts and pumping giving

$$S = (A_{ch}q_{ch} + A_{part}q_{part})/p_{base} \tag{6.7}$$

where q_{ch} and q_{part} are the specific outgassing rates of the chamber and part, respectively, expressed in pascal liter per second and meter squared.

Equation (6.7) quantitatively correlates pumping performance with chamber size (Fig. 6.2). The specific outgassing rates [20, 23] can vary by as much as an order of magnitude, depending on the material, cleanness, and history of the outgassing surfaces.

We will now consider examples of existing chambers used for tribological and semiconductor processing. We use the room temperature specific outgassing rates shown in Figure 6.13 [24] for materials that are typically used in PIII&D chambers. The outgassing data have been ranked as weak, nominal, and strong.

The first example is the large-scale, 3-m^3 HRL tribology facility [3] previously shown in exterior view in Figure 6.7 and in interior view in Figure 6.10. The chamber is constructed of type 316 stainless steel. The chamber was designed to have a base pressure of about 3×10^{-4} Pa. The total internal chamber area is 11 m^2, and the fixture table surface area is 2.8 m^2. Referring to Figure 6.13, we use the specific outgassing rate of about 5×10^{-2} Pa-l/s-m^2 after 2 h of pumping. Multiplying this specific outgassing rate by the total surface area, we obtain a total outgassing rate $A_{ch}q_{ch} + A_{part}q_{part} = 0.69$ Pa-l/s. Inserting this into Eq. (6.7), we find the pumping speed required to maintain a base pressure of about 3×10^{-4} Pa: $S = 2300$ l/s. In practice, the pump at the HRL chamber has an effective pumping speed of 2500 l/s.

As a second example, we evaluate the Northeastern University semiconductor processing facility [4]. The chamber is made of aluminum and has a total internal chamber area of 0.54 m^2. Referring to Figure 6.13, we use an average specific outgassing rate of 4×10^{-3} Pa-l/s-m^2 for aluminum after 1 h of

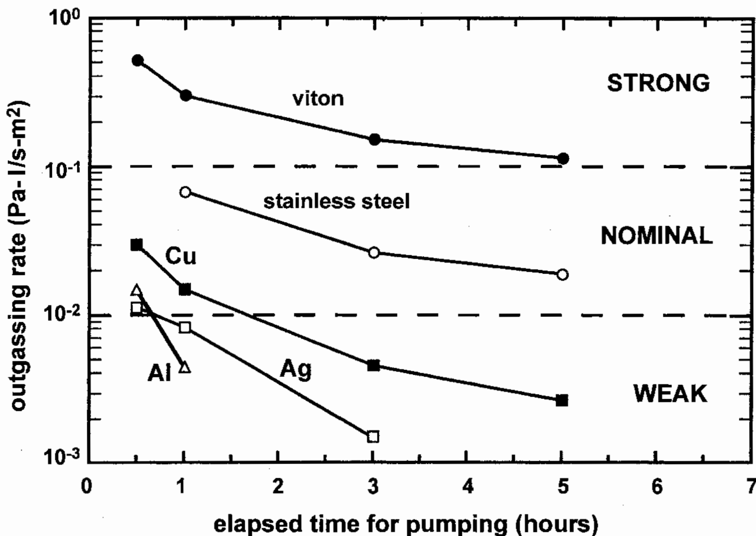

Figure 6.13 Room temperature outgassing rates of various materials used in PIII&D processing chambers.

pumping. The total outgassing rate of the chamber is expected to be $A_{ch}q_{ch} = 2.2 \times 10^{-3}$ Pa-l/s. With a base pressure of 5×10^{-4} Pa, Eq. (6.7) predicts that the high-vacuum pumping speed should have a value of $S = 4.4$ l/s. This pumping speed is in good agreement with the actual pumping speed of 4 l/s [4].

6.5.4 Determination of High-Vacuum Gas Throughput

The gas throughput requirement of a high-vacuum pump is given by Eq. (6.6). The pumping speed of the high-vacuum pump is approximately constant over a reasonable operating pressure range, typically until a pressure of about 0.1 Pa (1 mTorr) develops at the head of the high-vacuum pump [20, 25]. Its value is known from the analysis of the previous section. The operating pressure in the treatment stage must be known for a particular application before the gas throughput can be determined using Eq. (6.6). However, it is important to understand that the gas throughput value obtained from Eq. (6.6), Q_{op}, is *not* the maximum gas throughput capability of the high-vacuum pump, which is the quantity we seek. The maximum gas throughput should be at least twice the value of the working gas throughput obtained from evaluation of Eq. (6.6). To understand this, we must review the salient features of high-vacuum pump operation at the base pressure, Eq. (6.5), and at the operating pressure, Eq. (6.6).

Figure 6.14 shows the behavior of two high-vacuum pumps having different pumping speeds. This type of pump behavior is valid for any type of high-vacuum pump: oil diffusion pump, cryopump, or turbo-molecular pump, for example. For both pumping curves, the chamber pressure increases linearly according to Eq. (6.6) as the flow rate is increased. The slope of the pumping curves up to points A_2 and B_2, respectively, gives the inverse pumping speed, $1/S$. The operating points for the two pumps correspond to A_1 and B_1 for the cases of low and high pumping speeds, respectively. When the gas flow rate

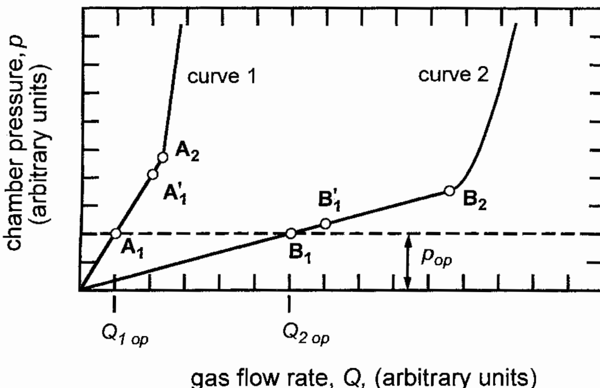

Figure 6.14 Variation of chamber pressure with gas flow rate for a processing chamber having two pumping speeds corresponding to curves 1 and 2.

increases to A_2 and B_2, the high-vacuum pumps choke or stall, that is, becoming ineffective in pumping gas. Each high-vacuum pump is then operating at its maximum gas throughput. For both pumps, the operating pressure, p_{op} is the same since this is a function of the PIII&D process and not of the pumping speed or gas throughput. Because of this, the operating gas throughput is less for the lower pumping speed (curve 1) than the operating gas throughput for the higher pumping speed (curve 2).

Now consider the chamber pumped by a high-vacuum pump of lower pumping speed (curve 1). The gas flow rate is set to Q_{1op}, corresponding to the operating point A_1. During an actual PIII&D treatment process, the gas flow rate remains constant; however, the total chamber pressure usually increases due to outgassing of the chamber walls or the parts treated. Note that the outgassing rate is higher than that considered in Section 6.5.2. Outgassing in the treatment stage is due to heating of the chamber walls and gas desorption stimulated by ion bombardment, ultraviolet photon, or electron impact, all effects caused by the PIII&D process itself.

If the chamber pressure is increased such as to operate the pump of curve 1 near its choking pressure, the success of the PIII&D process is in jeopardy because the system becomes unstable. The pump is inadequate to handle the changes in pressure caused by outgassing effects. Note that the species outgassed depend on the history of the outgassing surface and are not necessarily identical with the working gas but usually a mixture of water vapor, oxygen, carbon, carbohydrates, and the like.

If the chamber were operated with the higher pumping speed (curve 2 in Fig. 6.14), the pumping system design *would* be adequate. Consider that for the same amount of outgassing, the chamber pressure increases by only a small amount corresponding to the new operating pressure at point B'_1. Because of the higher pumping speed, this new operating pressure places the pump operation far from the choking point, and therefore the system is stable.

Often a throttling valve isolates the high-vacuum pump from the processing chamber. It allows the pumping speed (not the gas throughput) of the high-vacuum pump to be varied in order to cope better with different gas throughputs. One can change operation from curve 1 to curve 2 (Fig. 6.14), thus gaining an additional degree of freedom and ensuring the stability of the pressure required.

6.5.5 Types of High-Vacuum Pumps

Three types of high-vacuum pumps are used in PIII&D facilities: oil diffusion pumps, cryopumps, and turbo-molecular pumps. Each type of pump has characteristics that distinguish it from the others. These types of pumps are also used in conventional plasma processing done in physical vapor deposition (PVD) coaters [26] or plasma nitriding and carburizing chambers [27, 28].

Oil diffusion pumps are the simplest and cheapest approach to achieving high-vacuum conditions. They have high pumping speed that can meet nearly

any performance specification, and they have relatively low maintenance costs and high reliability. Oil diffusion pumps can pump all types of gases. Backstreaming of oil vapor can be controlled by using a liquid-nitrogen trap or refrigerated baffle above the head of the diffusion pump. However, trace amounts of oil are of concern in some high-tech applications. Trapping may be inadequate, thus disqualifying the use of diffusion pumps for these applications. Water vapor is best pumped using a cold trap or POLYCOLD refrigeration unit that can be easily incorporated into the diffusion pump stack assembly [20].

One disadvantage of oil diffusion pumps is that their operation is orientation dependent: The pump must be operated in a vertical configuration to keep oil in the bottom of the pump. Unless the pump can be mounted to a bottom port of the chamber, elbows are needed to couple the pump to the side of the chamber. The bottom mount requires vertical clearance that is often a serious issue for large-scale vacuum chambers. The use of elbows reduces the effective pumping speed (but not the gas throughput). Oil diffusion pumps offer a good combination of high performance and low cost for research, development, or commercial applications.

Two high-vacuum pumps that are not orientation dependent are the turbomolecular pump and the cryogenic pump. Cryopumps *are* oil free while turbopumps can be made to be completely oil free. Both of these pumps combine cleanness with high pumping speed and compactness, offering advantages over oil diffusion pumps.

The cryogenic pump is attractive because it can be mounted practically anywhere on the chamber. In a cryopump, gases that come in contact with the cold inner stage of the pump (about 12 K) condense there and are therefore removed (pumped) from the chamber. The pumping speed of cryopumps for water vapor is extremely high compared to diffusion pumps, however, for gases lighter than krypton, especially hydrogen, cryopumps have difficulty in pumping with high capacity. Particularly inefficient is the pumping of helium. Because of the cold trapping principle, a baffle should be used in PIII&D applications where high temperatures are experienced, such as in high-energy nitriding.

Unlike a diffusion pump or turbomolecular pump that is continuously exhausted by an auxiliary pump, the cryopump must be regenerated at regular intervals, especially when using high gas flow rates. To mitigate this, multiple cryopumps can be used in situations where down time due to pump regeneration is an issue. Regeneration occurs through degassing by a warm-up cycle. Frequent regeneration significantly affects the total cost of the system. Maintenance on cryopumps is higher than for oil diffusion pumps. However, cryopumps are an excellent choice for PIII&D processes with cathodic arc plasmas: Regeneration is very infrequent because processing is done at high vacuum.

Like the cryopump, the turbomolecular pump is compact in design and can be placed virtually anywhere on the chamber. Their advantage over cryopumps

is that they can pump all gases, including hydrogen and helium, and they do not require regeneration. The reliability of turbo pumps is quite acceptable, and they can be ganged (i.e., combined or grouped) to provide practically any pumping speed needed. In Table 6.2, the actual performance parameters for three typical high-vacuum pumps are compared: the Varian VHS-10 oil diffusion pump [25], the CTI Cryo-Torr 10 cryopump [29], and the Varian, Turbo-V1800 [25].

As an example we consider the HRL tribology facility shown in Figure 6.7. It was shown before that this facility was designed to have a base pressure of 3×10^{-4} Pa, corresponding to a required pumping speed for the high-vacuum pump of 2300 l/s for nitrogen (air). The maximum operating gas pressure required for PIII&D processes conducted in this facility is 0.4 Pa (3 mTorr) [17]. Using Eq. (6.6), this corresponds to a maximum operating gas throughput of 920 Pa-l/s (6.9 Torr-l/s). From the analysis in the previous section, the maximum gas throughput should be at least 1840 Pa-l/s (14 Torr-l/s), that is, twice the operating gas throughput. The HRL chamber has a single 10-inch (25.4 cm) and a single 8-inch (20.3 cm) flange port available for mounting of high-vacuum pumps. For the 10-inch port, the CryoTorr-10 cryopump listed in Table 6.2 was selected. It provides adequate pumping speed (3000 l/s at the exit of the pump and 2300 l/s at the chamber entrance past the gate valve), more than adequate maximum gas throughput capability. Most importantly, it is oil free and compact to fit in a small space. Figure 6.7 shows the CryoTorr-10 cryopump mounted on the right-side flange. The chamber is also equipped with two Balzers turbo-molecular pumps mounted in parallel on the 8-inch diameter flange (not shown in Fig. 6.7). The turbo pumps provide an additional 500 l/s pumping speed per pump for additional "safety-margin" pumping speed when the parts being treated outgas excessively. That is relevant for implantation operation at ~100 kW power levels where outgassing of the chamber walls

Table 6.2 List of pumping parameters and cost for three types of high-vacuum pumps

	High-Vacuum Pump		
Parameter	Oil Diffusion Varian VHS-10	Cryopump CryoTorr-10	Turbomolecular Varian V1800
Flange size (m)	0.254 ASA	0.254 ASA	0.254 ASA
Pumping speed (l/s)	5,300	3,000	1,600
Maximum gas throughput (Pa-l/s)	1000	2500	2100
Cost (thousands of dollars) (costs of vapor trapping not included)	10	20	27
Cost/(pumping speed) (thousands of dollars/l-s)	1.9	6.7	17

and parts can be very high. Additionally, these turbopumps pump gases that cannot be handled by the cryopump.

6.6 FIXTURES

6.6.1 Fixture Types

There are three types of fixture designs used in PIII&D. These are stationary, continuous linear feed, and rotating fixtures. These fixture designs are not unlike those used in conventional surface technology facilities, but they need to withstand the high voltages used in the PIII&D process.

As for conventional plasma carburizing or nitriding, stationary fixtures are routinely used when handling large dies and molds, and continuous linear feed fixtures are used for treating large numbers of small-scale components such as gears. In conventional PVD coating systems, rotating fixtures are routinely used to coat large numbers of small-scale tools and components [30, 31]. In existing PIII&D facilities, stationary fixtures are predominantly used, and this will be the focus of this section.

6.6.2 Design, Electrical Insulation, and Weight Capacity of Fixtures

Figure 6.2 lists the various elements that must be considered: structural design, weight capacity, electrical insulation capability. Additionally, active cooling or heating may be desired or required, but this is usually difficult to implement, in particular for three-dimensional parts. Three types of stationary fixtures are commonly used in PIII&D: single-support, multiple-support, and flat-table-support fixtures.

Figure 6.15 shows an example of a single-support stationary fixture used in the 1-m^3 GMR tribology facility. The high-voltage cable termination is mounted from the bottom of the chamber and extends into the chamber about 0.1 m, locating the part to be treated near the center of the chamber volume. The cable termination was fabricated of epoxy that can provide electrical insulation of 150 kV between the chamber wall and the end of the termination. The cable termination contains internal feed lines that can be used to actively cool the endplate and therefore the part that is placed on the endplate. The cooling achieved will depend on the size and type of part treated. The maximum operating temperature of the epoxy cable termination is about 100°C, so this fixture places constraints on the use for a high-temperature PIII&D process.

The single-support fixture serves the dual purpose of being the cable termination providing the electrical connection of the pulse modulator to the part being treated, as well as being the support for the weight of the part. This is acceptable for lightweights, however, as the part size or part number increases, a different approach is required.

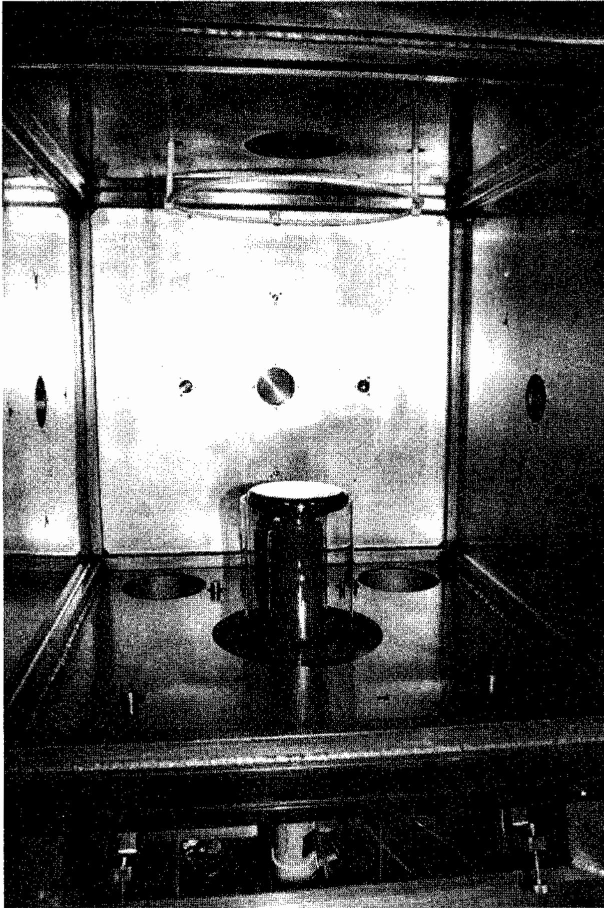

Figure 6.15 Photograph of the use of a single-support fixture used in the 1-m^3 tribology facility at General Motors Research.

One approach is the use of multiple single-fixtures with a single, separate high-voltage termination. Figure 6.16 shows an array of more than 1000 aluminum cylinders simulating aluminum automotive pistons [32]. The cylinders are mounted on water-cooled brackets that are supported and electrically insulated from the chamber walls using 8 ceramic standoffs as shown. The high-voltage termination to the array is accomplished by mounting a separate ceramic high-voltage (HV) feedthrough on the side of the chamber. The alumina standoffs are partially shielded (note the metallic cap between the support and the target assembly). The cap shields the upper portion of the support rod, significantly reducing the plasma density in this region, and allows PIII operation well in excess of 40 kV. Sputtering of metal from the substrate and other structures onto the surface of the insulators and HV feedthroughs is

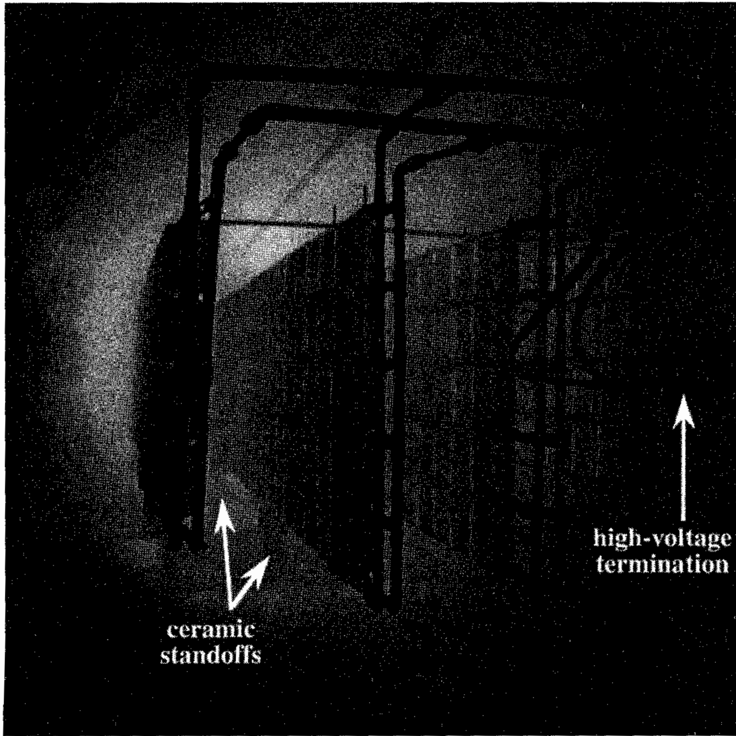

Figure 6.16 Use of multiple, single-support fixtures to support large numbers of parts in the LANL facility.

a problem because it can lead to arcing at the ceramic insulator–metal interface even at relatively low voltages. Metal coatings on high-voltage feedthroughs represent an additional, undesired, and uncontrolled load that in extreme cases can short-circuit the pulser voltage.

A second approach, shown in Figure 6.10, is the use of a flat-table-support fixture supported by ceramic standoffs [17]. A separate epoxy cable termination similar to that used in the single-support fixture in Figure 6.15 is realized through a flange mounting at the bottom of the chamber. It provides the electrical connection to the flat table without supporting the weight of the table and part.

Two sizes of support tables can be used in the facility shown in Figure 6.10 (only one of them is shown). For large loads of parts, a 1-m × 2-m support table is used with a maximum weight capacity of 3200 kg. For smaller loads, a 1-m × 1-m support table is used. Parts can be easily loaded and unloaded into the chamber manually or by forklift. The two support tables are fabricated of 6-mm-thick stainless steel. The large table is supported and isolated from the vacuum chamber walls using eight 5-cm-diameter, 15-cm-long alumina rods

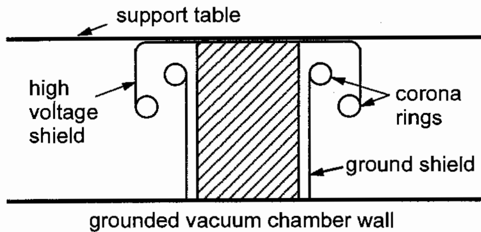

Figure 6.17 Schematic of the double-captured approach to shielding fixtures used in PIII&D systems.

that have aluminum corona ring mounts, as shown in Figure 6.10. The small table uses four alumina rods for support. The alumina rods provide for 400-kV direct current (DC) voltage insulation. The cable termination itself has a maximum voltage rating of 300 kV DC. Similar mounting arrangements are also used on the large-scale LANL facility shown in Figure 6.16. To provide plasma shielding and prevent coating of the cable termination and the ceramic standoffs, each of these elements can be enclosed in a double-captured, cylindrical tube, as shown schematically in Figure 6.17 [33].

Since semiconductor wafers are flat, the design of the sample stages is quite different from those used in tribological applications. For semiconductor processing, the stage should allow for in situ cooling (e.g., for hydrogen PIII in the ion-cut process) or heating (e.g., for oxygen PIII to synthesize SPIMOX). The common stage design consists of a flat plate made of material compatible with the process. In addition, the stage should have a dimension that ensures that ion dose and energy across the wafer surface are as uniform as possible [34, 35].

The examples given in the sections above for tribological and semiconductor processing applications have focused on fixture designs where the part temperature is not very high. In the case where the part temperature is intentionally high, such as in the case of high-energy nitriding ($T > 300°C$), flat support tables may be used if the part heating is predominantly from ion bombardment. Incorporating a heater into the table to provide separate control of the substrate temperature is only effective for flat parts. As discussed in the following section, a heat treatment furnace is required for three-dimensional parts.

6.7 TEMPERATURE CONTROL AND SHIELDING OF CHAMBER WALLS

6.7.1 Heating and Cooling of Chamber Walls

Temperature control of the chamber walls in a PIII&D facility is important for conducting low-temperature and high-temperature treatment of parts.

Secondary electrons emitted from an implanted part are accelerated across the plasma sheath surrounding the part. Unless they collide with gas molecules, which is likely only at high pressure, they impact the chamber walls with an energy equivalent to the full sheath voltage. If no active cooling of walls is used, electron impact causes heating of the chamber walls, which in turn may result in significant desorption of gases and materials that can prevent high-quality implantation. In the case of PIII nitriding, the use of auxiliary heaters on the walls of the chamber gives an additional degree of freedom to control the temperature of the part independent of the ion bombardment process.

If the mass of the chamber walls is large enough, heating of the chamber walls may be insignificant, in which case active cooling of the walls is not needed. This can be estimated by balancing the power of secondary electron heating on the one hand and rate of rise of the temperature of the walls and the rate of heat removal from the wall on the other hand. Duty cycle or average power of the pulser as well as duration of the treatment must be taken into account. Active cooling must be used if the chamber walls are not massive and the secondary electron power is significant.

External and internal cooling techniques of the chamber have been developed. In external cooling, water channels are welded to the exterior of the vacuum chamber wall. This approach has the advantage that it allows for direct contact of flowing water with the chamber wall maximizing the cooling effect. It has the disadvantage that one relies on the thermal conductivity of the chamber material to provide for heat flow between water channels. Since most chambers are fabricated of stainless steel, this may allow the temperature to be excessive at some locations since stainless steel has relatively poor heat conductivity. Another advantage of exterior channels is that the possibility of water leaks into the chamber is eliminated, which is obviously possible when using interior cooling. The advantage of internal cooling is that the heat is efficiently and almost instantaneously removed. A disadvantage is that water vapor condensed on the cooled chamber wall surfaces may desorb during treatment of parts, which may affect the quality of the implant.

The use of internal cooling panel hardware to dissipate secondary electron power is illustrated in Figure 6.10. The interior of the chamber has a dimpled, stainless steel shroud that extends over the upper hemisphere of the chamber. There is no shroud structure beneath the fixture table, nor on the front or rear of the chamber because secondary electrons are accelerated mainly into the upper hemispherical section of the chamber for a flat-fixture table design. Only very few secondary electrons are deposited beneath the fixture support. A dimpled shroud allows the water to be in direct contact with the shroud maximizing heat removal while also providing mechanical strength of the structure. The flow rate is about 40 l/min of process-cooled water, which is sufficient to dissipate 100 kW of secondary electron power for the water temperature not exceeding 50°C.

It should be noted that when using an internal shroud of any design, the venting and pumpdown procedure one normally follows must be modified to

eliminate water condensation on the shroud. This can be mitigated effectively by using a hot and cold water manifold that is sequenced to provide hot water (60°C) flow to the shroud during venting of the chamber to atmospheric pressure and initial stages of pumpdown. When the chamber pressure approaches low pressures (on the order of 10^{-3} Pa), the cooled process water is used.

6.7.2 PIII&D with Chamber Walls at Elevated Temperature

In the case of high-energy nitriding, the chamber wall needs to be able to cope with the heat load imposed on it by radiation from the workpieces. The vacuum chamber should be designed as a vacuum heat treatment furnace while plasma generation and high-voltage bias of the workpieces create some unique issues.

Two categories of vacuum heat treatment furnaces can be distinguished. In hot-wall furnaces, the heating elements are placed outside the vacuum retort and the chamber walls act as radiating elements transferring heat to the workpieces. Figure 6.18 shows a schematic diagram of a hot-wall furnace designed for PIII nitriding of components on an industrial scale, and Figure 6.19 shows a photograph of an actual system. From Figure 6.18, insulation material around the heaters reduces heat loss to the surrounding environment while thermal plugs at either end of the retort maintain a uniform temperature zone within the furnace. Only a relatively small amount of cooling is required on the end plates and around the O-rings used to seal the end plates.

In cold-wall furnaces, heating elements are placed right inside the vacuum chamber. The chamber walls are usually protected by heat shields or thermal

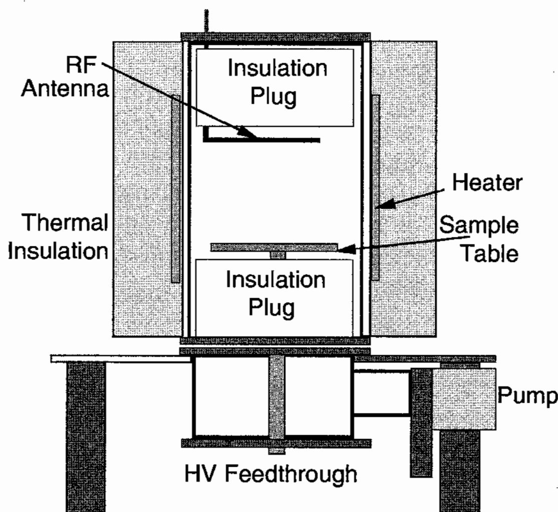

Figure 6.18 Schematic diagram of a hot-wall furnace for PIII nitriding of components.

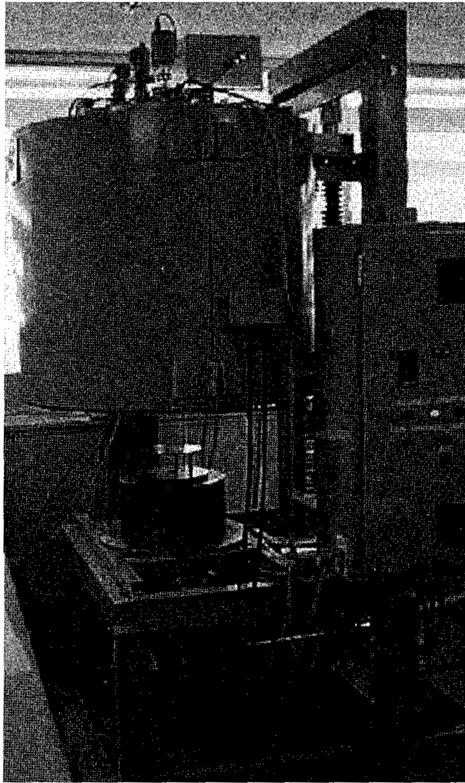

Figure 6.19 Photograph of a hot-wall furnace designed for PIII nitriding of components on an industrial demonstration scale.

packing, although the high-vacuum requirements of PIII&D would normally preclude the use of most insulation materials. In any case, the walls usually require cooling either by tubes welded on the outside of the chamber or by a double-wall arrangement with cooling water circulating between the two walls. The simplest realization of elevated temperature PIII&D [32, 36], in which ion bombardment is used to heat the workpieces, can be considered as a cold-wall furnace, although the lack of efficient cooling of the walls means that the chamber is often too hot to touch! By contrast, the outside case of a hot-wall furnace system remains at room temperature.

Although a cold-wall furnace may appear to be a simpler proposition at first sight, there are several disadvantages. The plasma may interfere with the heating elements and deposition on the heaters will cause problems. The heaters and their associated heat shields take up a significant portion of the vacuum chamber and increase the pumping capacity required to maintain the necessary base pressure. Although the heating effect of PIII&D must be dealt with in both systems, it is generally easier to maintain a uniform temperature

distribution in a hot-wall furnace. Most modern plasma nitriding units are based on hot-wall furnaces.

Figure 6.18 indicates how plasma generation [in this case using an immersed inductive radio frequency (RF) antenna] and high-voltage bias are achieved in a hot-wall furnace. They are introduced through the thermal plugs at either end of the retort. All components within the treatment zone are considered to be at temperature and no attempt is made to cool them.

6.7.3 Coating Protection by Internal Shields

An issue in all PIII&D facilities is maintaining clean chamber walls. The interior surface of the chamber is subject to deposition of materials and impurities during any PIII&D process but particularly those in which hydrocarbon gases or any other gas that contains nonvolatile constituents are used. Obviously, condensable plasmas from cathodic arc plasma sources are of particular concern. Deposition of sputtered or plasma material is an issue since these deposited materials can trap excessive amounts of gases and moisture during chamber openings. They desorb these gases during the process treatment stage and introduce unwanted contamination to the surface of the workpiece. In addition, material buildup on the chamber walls interferes with achieving the desired pumpdown time, base pressure, and required high-voltage insulation.

Maintenance of clean chamber walls is common to other surface technologies. For example, internal shields line the interior of conventional PVD chambers. These shields serve the purpose of protecting the actual vacuum chamber walls from being deposited with coatings. When a thick layer of material has been deposited onto the shields, a new clean set of shields is installed and the coated ones are cleaned for their next installation. As a rule of thumb, the internal shields used in coating chambers should be replaced every 20 cycles.

The use of interior shields in PIII&D chambers has been used for the same purpose as in PVD coating chambers. For PIII&D applications involving cathodic arc or similar plasmas, the use of shields is particularly important for the protection of electrical feedthroughs and windows. For the latter, vacuum carousel designs consisting of a barrel with several transparent shields (like quartz glass) are common. When one of these shields becomes opaque due to coating, a fresh one can be aligned on the vacuum side of the window. The shields can be "recycled" by etching the coatings periodically. An alternative approach is the use of a "venetian blind" shield that is installed on the vacuum side of the window. The blind shield is only opened when needed and otherwise closed, thus protecting the window from being coated.

Aluminum foil, stainless steel, and cold-rolled steel have been used for shielding purposes. Aluminum foil offers the advantage of simplicity, low cost, and ease in conforming it to curved surfaces of the interior parts of the chamber. However, aluminum foil easily tears and this makes it delicate to

handle and use. Stainless steel foils 250 to 750 μm thick (10 to 30 mil) mitigate this problem and allow for spot welding as a simple means of anchoring the foils to the chamber walls. Cold-rolled steel sheets have been used for internal shields, however, they easily rust, making long-term use an issue. Unlike aluminum foil and stainless steel, cold-rolled steel is magnetic and therefore can be used for dual purposes such as mounting of magnets for plasma confinement.

6.7.4 X-ray Shielding

The production of X-rays during PIII&D processes, their health hazards, and X-ray shielding are discussed in detail in Section 9.3.3. In this section we will only summarize elements affecting the design of the PIII&D chambers and discuss possible X-ray reduction techniques.

In one approach, the PIII&D vacuum chamber is completely wrapped with lead shielding of sufficient thickness to reduce the produced X-rays to safe levels. In a second approach, the PIII&D chamber is placed behind (sometimes movable) lead curtains or in a lead or concrete processing room that is separated from the control room occupied by personnel.

An example of the first approach used for X-ray shielding is illustrated in Figure 6.7. The exterior of the chamber has a conformal covering of four layers of 1.6 mm thick ($\frac{1}{16}$ inch) lead for a total thickness of 6.4 mm ($\frac{1}{4}$ inch). This shielding is sufficient to allow for safe, stable, continuous operation at a voltage of 100 kV and power of 100 kW (Section 9.3.3). The top of the chamber shown in Figure 6.7 has a rectangular lead-shielded box for additional shielding of the plasma source vacuum ports, ionization gage access ports, and gas feedlines. Additionally, the sides, front, and rear of the vacuum chamber have lead-covered, cylindrical caps that are easily removable, as shown, to cover the high-vacuum pump and other access ports to the chamber. Protective paints can be used to prevent lead poisoning when touching the shields with hands.

Two advanced processing techniques have been explored for X-ray mitigation or reduction. One of them has been reduced to practice. Both techniques deal with suppression of secondary electrons from impacting the chamber walls to produce X-rays. These two techniques are described in Section 4.3. Here we show how the hardware is implemented into an actual facility.

The first technique uses electrostatic confinement of secondary electrons (Fig. 4.11) [37, 38]. A metal enclosure is placed at the perimeter of the chamber and held at the same potential as the part and the fixture. A ground-potential, remote plasma source is used to produce ground-potential plasma inside the enclosure that is used as the source of ions.

Figure 6.20 shows a photograph of a stainless steel enclosure that was fabricated to demonstrate the electrostatic confinement approach, using the chamber shown in Figure 6.7. The enclosure has a 20.3-cm-diameter hole in the top of the enclosure for entry of the cylindrical, remote plasma source that is

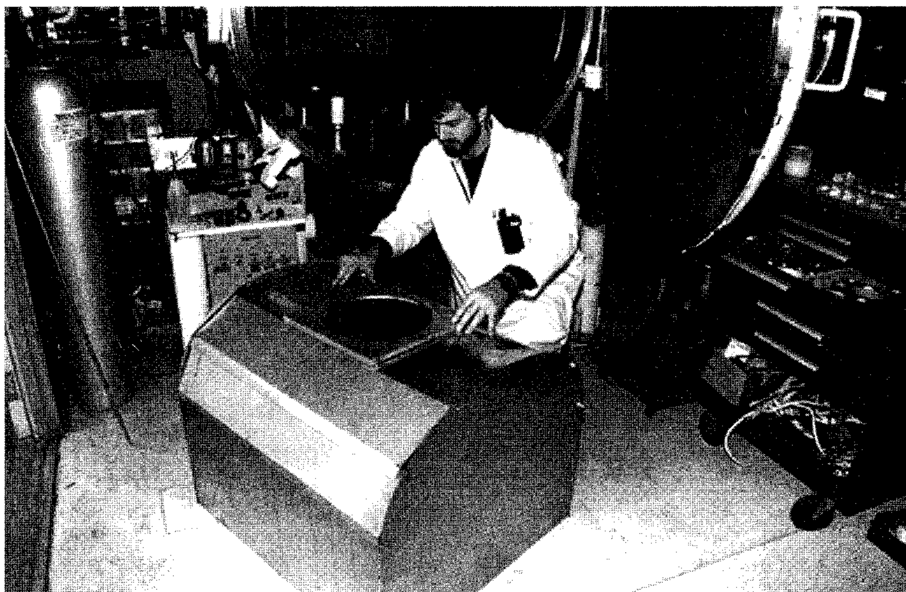

(a)

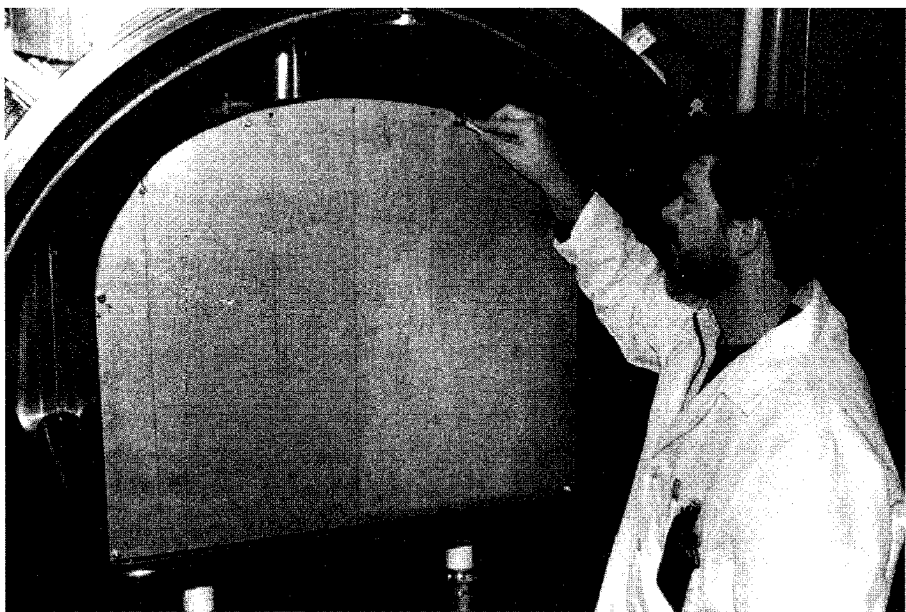

(b)

Figure 6.20 Photograph of stainless steel enclosure (*a*) before and (*b*) after placement into the 1.2-m-diameter HRL chamber for X-ray reduction.

mounted directly on the vacuum chamber. The enclosure rests on the flat table fixture, to ensure that it is at the same potential as the table. Figure 6.20*b* shows the enclosure installed in the chamber.

A second but yet-untested technique for suppressing secondary electrons is to make use of an externally applied magnetic field oriented along the length of the part [39]. Secondary electrons emitted from the part are trapped in the field to form a virtual cathode layer near the part surface, where the local electric field is substantially reduced. Figure 1.13 is a photograph of the Los Alamos National Laboratory tribology facility with eight magnetic-field coils arranged to provide an axial magnetic field that can be used to reduce this proposed approach to practice [32].

6.8 PROCESS DIAGNOSTICS AND CONTROL

6.8.1 In Situ Diagnostics

There are numerous diagnostic methods available to the PIII&D technologist. Among them are pre- and posttreatment diagnostics as well as in situ diagnostics. Pretreatment and posttreatment diagnostics are used to characterize the part's surface outside the PIII&D chamber (Chapter 5). In contrast, in situ diagnostic hardware is mounted directly to the vacuum chamber and will be summarized here.

In situ diagnostics are important to ensure repeatability, consistency, and quality of the PIII&D process. Diagnostics presently used include plasma probes to measure plasma parameters, current and voltage probes to measure the ion and electron constituents incident on the substrate, dose measurements, and temperature measurements.

Langmuir probes and other techniques are routinely used to measure and monitor properties of the various species in the plasma. The reader is referred to a host of techniques described in detail in the literature (e.g., [40, 41]). Langmuir probes can be used to obtain ion and electron densities, electron temperature, and plasma potential. They cannot, however, identify the species and charge state of ions. This information is obtained using a high-sensitivity charge-to-mass analyzer. In addition to measuring ion species, a high-sensitivity mass analyzer can also operate in the residual gas analyzer (RGA) mode to monitor the various neutral gas species.

Plasma spectroscopy is a powerful tool for identifying species and monitoring relative population and species densities. Sophisticated techniques have been developed for the interpretation of spectroscopic, data but quantitative analysis is often difficult and requires calibration by other techniques.

Optical (or infrared) pyrometry is often routinely used for the determination of temperatures of surfaces such as hot workpieces and electrodes. The

emissivity (ε value) of the infrared (IR)-emitting surface and the transmittance of the windows must be known or taken into account.

In situ ellipsometry can be used to the measure film thickness while the film is still growing by the PIIID process. A disadvantage is that sophisticated and expensive equipment is needed. An alternative method relies on measuring changes to the frequency of a calibrated quartz crystal. However, temperature effects and electrical insulation from the PIII&D high voltage are difficult issues.

6.8.2 Process Control of a PIII&D Facility

There are a number of alternatives for control of a PIII&D facility ranging from personal computer (PC)-based interface boards with a software package such as LabVIEW™ to versatile module eurocard (VME)-based industrial control systems operating under high-level operating systems. The most important feature, however, is that the various subsystems (vacuum, gas control, plasma generation, high voltage, heaters) be integrated into a single system [36]. Programmable logic controllers (PLCs) have become a very popular solution in modern industrial practice. Control is implemented in external PLC units and dedicated temperature controllers that handle process and vacuum system management, maintenance of interlocks, regulation of process parameters, and automated process sequencing. Operator interface, alarm monitoring, and data logging can be handled by an industry standard SCADA (Supervisory, Control and Data Acquisition) package on a PC. Communication between PC and external units is usually via serial links using RS-232 or RS-485 communication standards or by dedicated PLC communication buses. This separation of control from supervisory and monitoring functions between PLC and PC has wide industry acceptance, ensuring reliable operation, independent of the PC. It is also highly flexible, facilitating machine and process development in addition to improvement of the monitoring functions.

Operation of the high-voltage pulse circuitry, which is the least familiar part of the system to industry users, has to be made as transparent as possible by its integration into the control system [36]. Although the pulse modulator generates fast variables, specific interfaces can be used to generate slowly varying signals for pulse voltage, current, frequency, and dose. These signals can be monitored by the PLC and logged by the PC in the same way as other treatment parameters such as flow, pressure, and temperature.

If collisions of ions in the sheath can be neglected, measurement of the high-voltage bias can be used to determine the ion energy. More than one ion energy is present if multiple ion charge states are present (Section 4.8).

Measurements of the dose of implanted ions are more difficult. Although there is ion bombardment on all exposed surfaces of the substrate, there are variations in the local ion current density due to the shape of the components.

The ion current density and hence implantation dose is greater near corners and edges while cavities will receive lower doses (Section 4.5). For *low* implantation doses ($D \ll 10^{17}$ ions / cm^2), the average retained dose is not much smaller than the incident dose (fluence), and it can be estimated by

$$D = \frac{f\,\Delta t\, I_p t}{\bar{Z}e(1 + \gamma_{SE})A} \tag{6.8}$$

where f is the pulse repetition frequency, Δt is the duration of one bias pulse (i.e., $\delta = f\Delta t$ is the bias duty cycle), t is the processing time, I_p is the pulser current (during each pulse), A is the exposed surface area of the substrate, and γ_{SE} is the secondary electron yield at the ion energy (which is determined by bias voltage and mean ion charge state, $\bar{Z}$). Equation (6.8) fails to represent the retained dose when the fluence is high because previously implanted ions become sputtered (the issue of retained dose limitation has been discussed in Sections 4.5 and 4.8.3).

An important issue for the practical use of Eq. (6.8) is the often-unknown secondary electron yield γ_{SE}. The literature contains a number of measurements of γ_{SE} for particular materials and particular ions within restricted energy ranges. However, most of them are of little value to PIII&D. One approach is a simple power balance measurement as suggested in [42]. The estimates of γ_{SE} obtained in this way are significantly lower than those obtained by ion beam irradiation of surfaces under vacuum condition. They show less variation across the range of materials usually treated by PIII&D. Collins and co-workers [43] have published values of γ_{SE} for a number of gaseous species suitable for use in PIII&D. More details are discussed in Section 4.3.

While the high-voltage pulse amplitude and the integrated dose are important process parameters when PIII&D is used for ion implantation, the treatment time and temperature are vital parameters for high-energy ion nitriding. Measurement of the temperature of the workpiece is complicated by the high-voltage bias applied during the process. Collins and co-workers [36, 43] used one-color and later two-color infrared pyrometers in the range 2.0 to 2.6 μm. For instance, one can use a single-color infrared pyrometer to view a point of calibrated emissivity on the substrate through a quartz window. A cavity in the substrate support is used as a reliable reference point for maintaining constant emissivity. Calibration is obtained by separately heating the target with thermocouples inserted. The effective emissivity of this cavity as seen by the pyrometer is around 0.72, mainly due to absorption in the quartz window. Temperature variations across the target components are difficult to monitor with a single-color pyrometer. This can be mitigated by using a two-color pyrometer. The temperature as monitored by a pyrometer can easily be maintained to within ±1°C by regulating the duty cycle of the high-voltage bias or the power to auxiliary heaters using the pyrometer output as input to a PID control loop.

REFERENCES

1. B. P. Wood, I. Henins, R. J. Gribble, W. A. Reass, R. J. Faehl, M. A. Nastasi, and D. J. Rej, "Initial operation of a large-scale plasma source ion implantation experiment," *J. Vac. Sci. Technol. B* **12** (1994), 870–874.
2. P. K. Chu, S. Qin, C. Chan, N. W. Cheung, and K. K. Ping, "Instrumental and process considerations for the fabrication of silicon-on-insulators (SOI) structures by plasma immersion ion implantation," *IEEE Trans. Plasma Sci.* **26** (1998), 79–84.
3. J. N. Matossian and D. M. Goebel, "Design characteristics of a 100 kV, 100 kW plasma ion implantation facility," *Surf. Coat. Technol.* **85** (1996), 86–91.
4. S. Qin and C. Chan, "Plasma immersion ion implantation doping experiments for microelectronics," *J. Vac. Sci. Technol. B* **12** (1994), 962–968.
5. G. W. Malaczynski, A. H. Hamdi, A. A. Elmoursi, and X. Qui, "Ion implantation and diamond-like coatings of aluminum alloys," *J. Mater. Eng. Performance* **6** (1997), 223–239.
6. R. Hutchings, G. A. Collins, and R. Tendys, "Plasma immersion ion implantation—duplex layers from a single process," *Surf. Coat. Technol.* **51** (1992), 489–494.
7. A. Anders, "Metal plasma immersion ion implantation and deposition: A review," *Surf. Coat. Technol.* **93** (1997), 157–167.
8. R. J. Adler, J. Scheuer, and W. Horne, "Thyratron modulators in plasma source ion implantation," paper presented at the Tenth IEEE International Pulsed Power Conference, Digest of Technical Papers, Albuquerque, NM, 1995, pp.1243–1248.
9. R. J. Adler, North Star Research, Albuquerque, NM, personal communication, 1998.
10. V. I. Khvesyuk and P. A. Tsygankov, "The use of a high-voltage discharge at low pressure for 3D ion implantation," *Surf. Coat. Technol.* **96** (1997), 68–74.
11. R. Günzel, E. Wieser, E. Richter, and J. Steffen, "Plasma source ion implantation of oxygen and nitrogen in aluminum," *J. Vac. Sci. Technol. B* **12** (1994), 927–930.
12. S. M. Malik, K. Sridharan, R. P. Fetherston, A. Chen, and J. R. Conrad, "Overview of plasma source ion implantation research at University-of-Wisconsin-Madison," *J. Vac. Sci. Technol. B* **12** (1994), 843–849.
13. B. Mizuno, I. Nakayama, M. Takase, H. Nakaske, and M. Kubota, "Plasma doping for silicon," *Surf. Coat. Technol.* **85** (1996), 51–55.
14. T. Sheng, S. B. Felch, and C. B. Cooper, "Characteristics of a plasma doping system for semiconductor device fabrication," *J. Vac. Sci. Technol. B* **12** (1994), 969–972.
15. X. Y. Qian, M. H. Kiang, J. Huang, D. Carl, N. W. Cheung, M. A. Lieberman, I. G. Brown, K. M. Yu, and M. I. Current, "Plasma immersion Pd ion implantation seeding pattern formation for selective electroless Cu plating," *Nucl. Instrum. Methods Phys. Res. B* **55** (1991), 888–892.
16. P. K. Chu, X. Lu, S. S. K. Iyer, and N. W. Cheung, "A new way to make SOI wafers," *Solid State Technol.* **40** (1997), S9–S14.
17. J. N. Matossian and R. H. Wei, "Challenges and progress toward a 250 kV, 100 kW plasma ion implantation facility," *Surf. Coat. Technol.* **85** (1996), 111–119.

18. J. N. Matossian, "Plasma immersion ion implantation technology at Hughes Research Laboratories," *J. Vac. Sci. Technol. B* **12** (1994), 850–853.
19. M. Tuszewski, J. T. Scheuer, I. H. Campbell, and B. K. Laurich, "Plasma immersion ion implantation for semiconductor thin film growth," *J. Vac. Sci. Technol. B* **12** (1994), 973–976.
20. M. H. Hablanian, *High Vacuum Technology: A Practical Guide* (New York: Marcel Dekker, 1990).
21. D. M. Hoffman, B. Singh, and J. H. Thomas III, Ed., *Handbook of Vacuum Science and Technology* (San Diego, CA: Academic, 1998).
22. J. M. Lafferty, Ed., *Foundations of Vacuum Science and Technology* (New York: Wiley, 1998).
23. J. F. O'Hanlon, *A User's Guide to Vacuum Technology*, 2nd ed. (New York: Wiley, 1989).
24. Leybold, *Leybold Product and Vacuum Technology Reference Book* (Export, PA: Leybold, 1998).
25. Varian, *Varian Products Catalog* (Lexington, MA: Varian, 1998).
26. R. F. Bunshah, Ed., *Deposition Technologies for Films and Coatings: Science, Technology, and Applications* (Park Ridge, NJ: Noyes, 1994).
27. L. McCrary, Dynavac, personal communication, 1995.
28. D. Goodman, Surface Combustion, Maumee, OH, personal communication, 1992.
29. CTI, *Products Catalog of Helix Technology Corporation* (Waltham, MA: CTI Cryogenics, 1998).
30. W. D. Munz, "The unbalanced magnetron—current status of development," *Surf. Coat. Technol.* **48** (1991), 81–94.
31. J. Matossian, R. H. Wei, J. Vajo, G. Hunt, M. Gardos, G. Chambers, L. Soucy, O. D., L. Jay, C. M. Taylor, G. Alderson, R. Komanduri, and A. Perry, "Plasma-enhanced, magnetron-sputtered deposition (PMD) of materials," *Surf. Coat. Technol.* **109** (1998), 496–506.
32. C. P. Munson, R. J. Faehl, F. Henines, M. Nastasi, W. A. Reass, D. J. Rej, J. T. Scheuer, K. C. Walter, and B. P. Wood, "Recent advances in plasma source ion implantation at Los Alamos National Laboratory," *Surf. Coat. Technol.* **84** (1996), 528–536.
33. R. Brunke, Empire Hard Chrome, Chicago, IL, personal communication, 1998.
34. Z. N. Fan, P. K. Chu, C. Chan, and N. W. Cheung, "Sample stage induced dose and energy nonuniformity in plasma immersion ion implantation of silicon," *Appl. Phys. Lett.* **73** (1998), 202–204.
35. D. T. K. Kwok, P. K. Chu, and C. Chan, "Ion dose uniformity for planar sample plasma immersion ion implantation," *IEEE Trans. Plasma Sci.* **26** (1998), 1669–1679.
36. G. Collins, R. Hutchings, K. T. Short, J. Tendys, and C. H. van der Valk, "Development of a plasma immersion ion implanter for the surface treatment," *Surf. Coat. Technol.* **84** (1996), 537–543.
37. J. N. Matossian and J. D. Williams, "Confinement of secondary electrons in plasma ion processing," U.S. patent 5,498,290, Hughes Aircraft Company, 1996.

38. D. J. Rej, R. J. Faehl, and J. N. Matossian, "Key issues in plasma-source ion implantation," *Surf. Coat. Technol.* **96** (1997), 45–51.

39. D. J. Rej, B. P. Wood, R. J. Faehl, and H. H. Fleischmann, "Magnetic insulation of secondary electrons in plasma source ion implantation," *J. Vac. Sci. Technol. B* **12** (1994), 861–866.

40. W. Lochte-Holtgreven, Ed., *Plasma Diagnostics* (New York: American Institute of Physics, 1995). Reprint of the 1968 edition by North-Holland, Amsterdam.

41. R. H. Huddlestone and S. L. Leonard, Ed., *Plasma Diagnostic Techniques* (New York: Academic, 1965).

42. J. P. Blanchard, "Target temperature prediction for plasma source ion implantation," *J. Vac. Sci. Technol. B* **12** (1994), 910–917.

43. G. A. Collins, K. T. Short, and J. Tendys, "Characterisation of high voltage pulser performance in radiofrequency plasmas," *Surf. Coat. Technol.* **93** (1997), 181–187.